Abstract

Ras proteins are small (~21kD) guanine nucleotide binding proteins (G-proteins) that are part of a large (>150) superfamily of GTPases. Three (K-, H- and N-) Ras isoforms encode 4 Ras proteins. They function as molecular switches, that cycle between inactive GDP- and active GTP-bound states to control cellular growth. About 30% of all cancers contain single point mutations in Ras that induce its chronic activation.[1] Of the three isoforms, K-Ras is mutated at the highest frequency in human cancer. The K-Ras^{G12C} mutation, in particular, is found in about 33% of non-small cell lung carcinomas.[2] Recent studies have targeted the K-Ras^{G12C} mutation for drug discovery utilizing cysteine-reactive small molecules, which will soon be the first Ras inhibitors to move to stage-1 clinical trials.[3] This project investigated a new small molecule candidate, naringenin, that binds in the same pocket as the K-Ras^{G12C} inhibitors. The binding site and affinity of naringenin to K-Ras^{G12C} was evaluated using 2D Heteronuclear Single Quantum Coherence (HSQC) spectroscopy. Our findings indicate that naringenin binds weakly to an allosteric pocket near the switch-II region of K-Ras^{G12C} and induces changes in guanine nucleotide exchange. The addition of an acrylate group to naringenin allowed for an irreversible bond to form between naringenin and cysteine-12 to overcome low affinity. This “warhead” inhibitor candidate can be modified further to bind tighter within the allosteric pocket of Ras. Furthermore, we find that a subset of selective estrogen receptor modulators (SERMs) which share similar characteristics to naringenin, bind in the same pocket, and may provide for an additional direction for Ras drug development.

Introduction

Ras proteins function as molecular switches to regulate cellular growth. When activated in response to upstream receptors, they transduce signals to multiple downstream pathways. The mitogen-activated protein kinase (MAPK) cascade, is a key Ras-mediated pathway, which transmits signals for the transcription of genes that control cell growth and division.[5] Ras adopts two states to determine its activity: an on-state and an off-state.[6] Ras is in its off-state when it is bound to GDP and is in its on-state when it is bound to GTP. The binding affinity of several effector proteins depend on the nucleotide bound-state of Ras. GTP binding induces a conformational change in the Ras switch-I (residues 30-37) and switch-II (60-76) regions.[3] Effector proteins bind to the GTP-bound Ras with a higher affinity relative to the GDP-bound state. Ras proteins possess low intrinsic GTP-hydrolysis activity which is regulated by GTPase Activating Proteins (GAPs). GAPs downregulate Ras activity by hydrolyzing GTP that is bound to Ras, changing Ras to its off-state and decreasing the effector binding affinity of switch-I and switch-II. Guanine nucleotide Exchange Factors (GEFs) upregulate Ras activity by exchanging GDP for GTP, changing Ras to its on-state and increasing its binding affinity to effectors. Most oncogenic mutations of Ras lead to the chronic activation of Ras by decreasing GAP-mediated GTP hydrolysis.[1] The decrease in GAP activity leads to an increase in the population of Ras that is GTP bound and activated in cells. Ras mutations that negatively affect GAP binding or increase the GEF mediated exchange of GDP to GTP lead to a chronic activation of Ras that causes the deregulation of cell proliferation and the formation of tumors.[1]

The most prevalent site of mutation in K-Ras is at position 12. A mutation of the K-Ras glycine residue at amino acid position 12 to a cysteine has been studied recently for its potential as a site

for attack by cysteine-reactive small molecules.[3] These small molecules contain strong electrophile chemical groups that create an irreversible bond with the cysteine due to its nucleophilicity within a biological pH range. Previous work by the Shokat group has shown that a new line of K-Ras^{G12C} inhibitors that bind irreversibly to the reactive cysteine show promising results by inhibiting K-Ras^{G12C} from adopting an active state.[3] New generations of K-Ras^{G12C} inhibitors continue to be explored as while it is at the forefront of Ras drug discovery research.[4] These inhibitors of K-Ras^{G12C} are unique in that they associate with Ras in an allosteric pocket of the switch-II region, irreversibly ligate the reactive cysteine of K-Ras^{G12C}, do not bind wild-type K-Ras with appreciable affinity.

The purpose of this project was to develop a new K-Ras^{G12C} inhibitor that binds to the induced allosteric pocket in the switch-II region with high affinity. The preliminary objective was to determine whether naringenin is a suitable molecular starting-point to develop further into an inhibitor that irreversibly binds the K-Ras^{G12C} cysteine. This investigation employed the use of NMR spectroscopy, fluorescence reactivity and nucleotide exchange assays. Through this research, we hope to gain insight on the proper optimization of K-Ras^{G12C} inhibitors and to eventually pave a way for the development of inhibitors for other K-Ras mutations.

Experimental Setup

Characterization of naringenin binding required successful expression and purification of K-Ras^{G12C} within a non-oxidizing environment to preserve the reactivity of its cysteine at the 12th amino acid residue. The recombinant DNA for K-Ras^{G12C} was synthesized and its sequence confirmed by Guowei Yin before its expression. The K-Ras^{G12C} vector, containing a 6x His-tag (~1 kDa) and TEV cleavage domain (~4 kDa) was transformed, cultured, and induced via IPTG. The purification process included reducing agent in order to ensure that the reactive cysteine at amino acid position 12 would not oxidize or dimerize. The protein was purified under reducing conditions on a His-tag nickel column and the purity was confirmed with SDS-PAGE. The His-tag was cleaved off by the use of Tobacco Etch Virus (TEV) protease. The yield of purified protein was measured using UV-spectroscopy. Sodium azide was added to protein for short-term storage at 4°C to prevent bacterial growth. The protein was diluted to 50% glycerol and sodium azide was added for long-term storage at -20°C.

Nucleotide exchange assays were performed using fluorescently labeled guanine nucleotides. The Mant fluorophore was used to visualize the exchange of guanine nucleotide. Two samples of K-Ras^{G12C} were loaded with Mant-GDP and Mant-GMPPCP, a non-hydrolysable analogue of Mant-GTP due to its carbon bond between the secondary and tertiary phosphates. Mant-GDP loading inactivated Ras, and Mant-GMPPCP loading activated Ras. The overexpressed K-Ras^{G12C} sample was preloaded with GDP upon purification. Free GDP was added to exchange with the loaded Mant-nucleotide to induce and measure decay in fluorescence associated with Mant-nucleotide dissociation. Free Mant-nucleotide was added to exchange with GDP that was loaded on K-Ras^{G12C} to induce and measure growth in fluorescence associated with Mant-nucleotide association. The Mant-nucleotide dissociation and association constants were then calculated. Subsequent assays were performed with the addition of naringenin at different relative concentrations to K-Ras^{G12C} to observe the effects of naringenin on nucleotide exchange. Similar assays were performed on UNC-5700 ligated K-Ras^{G12C}.

^{15}N isotope labeled K-Ras^{G12C} was prepared for HSQC spectroscopy experiments. The *E. coli* cell growth was in the presence of ^{15}N isotope labeled ammonium chloride. Once purified, the labeled protein was exchanged into NMR buffer. CSP data was measured from 2D NMR HSQC data. The ^{15}N and ^{1}H peaks were normalized and the CSPs were calculated using the following equation: $CSP = \sqrt{\frac{(\partial_{N,G12C+Compound-N} - \partial_{N,G12C})^2}{25} + (\partial_{H,G12C+Compound-N} - \partial_{H,G12C})^2}$ (Equation 1).

K-Ras^{G12C} was reacted with the naringenin-warhead, UNC-5700, in the presence of ethylenediaminetetraacetic acid (EDTA) and 2-mercaptoethanol (2-ME). The buffer contained equimolar $MgCl_2$ and EDTA and equimolar 2-ME and UNC-5700. A ratio of 1:100 protein to ligand (K-Ras^{G12C} : UNC-5700) was used. The reaction was left for two hours at room temperature. The sample was buffer-exchanged to remove any excess or unreacted UNC-5700.

Methods and Protocols

Constructs. The human cDNA sequence that encodes the G-domain of each Ras mutant (C118S and G12C cysteine-light, residues 1-169) was subcloned into a pET21 vector. The human cDNA that encodes the SOS1 gene (SOS^{cat}) was subcloned into a pQlinkH vector (residues 550-1050). Both vectors add a TEV protease cleavage site and N-terminal 6x-histidine tag to the sequence.

Bacterial Transformation. 1.2 µL of K-Ras^{G12C} recombinant DNA was added to 30 µL of BL21(DE3) RipL competent cells. The cells were incubated on ice for 30 minutes before being heat shocked at 42°C for 45 seconds. Then, the cells were incubated on ice for an additional 2 minutes. The cells were plated on LB Agar plates that contained Ampicillin and Chloramphenicol antibiotics. The plates were incubated at 37°C for 20 hours.

Bacterial expression. 1 L of LB media (10g tryptone powder, 5g yeast extract, 10g NaCl, 1 L ddH_2O) was autoclaved in a 2.5 L shaker flask. Starter cultures were made with 40 mL of previously autoclaved LB media in 250 mL autoclaved shaker flasks. To the 250 mL shaker flasks, 40 µL of 1000x Ampicillin and 1000x Chloramphenicol were added. Then, one colony from the LB Agar plate was added with the use of a flame sterilized inoculating loop. The starter cultures were grown overnight at 25°C and 225 rpm. The OD_{600} was measured the next day. Once the growth grew to an OD_{600} of 1.0 or greater, the starter cultures were transferred to a centrifuge tube and the sample was centrifuged for 10 minutes at 3800 rpm. The supernatant was poured off and the pellet was resuspended in LB media from a 2.5 L shaker flask that contained 1 L LB, 1 mL of 1000x Ampicillin and 1000x Chloramphenicol. The 2.5 L shaker flasks were then incubated at 37°C and 225 rpm for 3-4 hours. The OD_{600} was checked periodically until the OD_{600} reached 0.55, at which time the flasks were incubated on ice for 10 minutes. The shaker temperature was set to 18°C during this incubation. After 10 minutes on ice, 800 µL of 0.5 mM IPTG was added to each flask to initiate transcription and translation of the recombinant DNA. Then, the flasks were returned to the shaker to incubate at 18°C and 175 rpm overnight. The next day, the growth was collected and centrifuged at 4000 rpm for 25 minutes. After discarding the supernatant, the pellet was resuspended in 35 mL of Wash Buffer A (20 mM HEPES, 300 mM NaCl, 5 mM $MgCl_2$, 20 mM imidazole, 10 µM GDP, 0.5 mM TCEP, 5% glycerol, pH 7.75). The cell growth was stored at -20°C.

NMR experiments expression of uniform 15N-enriched Ras. M9 minimal media was used to grow cells with ^{15}N isotope enriched K-Ras^{G12C}, and was prepared by autoclaving the following: 100 mL of 10x M9 salts at pH 7.4, 885 mL of ddH_2O. After autoclaving, the following was added to the media: 1.0 g of $^{15}NH_4Cl$, 1 mL each of 1000x Ampicillin and 1000x Chloramphenicol, 500 µL of 1.0M $CaCl_2$, 2.0 mL of 1.0 M $MgSO_4$, 168 µL of 0.3 M $ZnSO_4$, 6.0 g of D-Glucose, 90 mg of thiamine, and 10 mL of 100x sterile-filtered vitamins (5 mg biotin, 5 mg choline chloride, 5 mg folic acid, 5 mg niacinamide, 5 mg D-pantothenate, 5 mg pyridoxal, 0.5 mg riboflavin, in 50 mL ddH_2O). The steps above for growth, incubation, and collection remain the same.

Ras Purification. The purification of 6x-His-tagged K-Ras^{G12C} involved the use of nickel column affinity chromatography. The reducing agent tris(2-carboxyethyl)phosphine (TCEP) was added to a concentration of 2.5 mM for each step of the purification. Two 35 mL cultures of previously collected growth were thawed and combined in a sonication beaker. Two complete ULTRA Tablets (inhibitor cocktail) were dissolved in 70% ethanol and added to the sonication beaker. The sonication beaker was placed in an ice bucket filled with ice and water and sonicated for 18 minutes with a 5-second on and 5-second off pulse cycle. After sonication, the sample was transferred to centrifuge tubes and centrifuged for 25 minutes at 16,000 rpm.

Before purification, the nickel bead column was washed with 35 mL of Elution Buffer (15 mM HEPES, 50 mM NaCl, 5 mM $MgCl_2$, 250 mM imidazole, 10 µM GDP, 0.5 mM TCEP, pH 7.75) and 100 mL of ddH_2O. Then, the column was equilibrated with 50 mL of Wash Buffer A. The supernatant from the centrifuge tube was transferred to the column and the flow through was collected. 21 µL samples from the lysate, pellet, and flow through were collected and mixed with 7 µL of reducing dye for an SDS-PAGE gel run. The column was then washed sequentially with 50 mL of Wash Buffer A, 50 mL of Wash Buffer B (20 mM HEPES, 1 M NaCl, 5 mM $MgCl_2$, 40 mM imidazole, 10 µM GDP, 0.5 mM TCEP, 5% glycerol, pH 7.75), and 50 mL of Wash Buffer A. Samples were taken from each wash as well and mixed with reducing dye for the SDS-PAGE gel run. Elution buffer was then added in 25 mL increments to the column to initiate the elution of K-Ras^{G12C}. The elution of protein was monitored taking a 35 µL sample of the dropping eluate and adding it to 900 µL of Bio-Rad protein assay dye. Elution buffer was added in 25 mL increments until the eluate samples no longer caused a color change in the Bio-Rad protein assay dye. A sample of the protein elution was taken and mixed with reducing dye for the SDS-PAGE gel run.

The column was then washed with an additional 35 mL of Elution Buffer, 50 mL of ddH_2O, and stored with ddH_2O at 4°C. The protein was then transferred to a dialysis tubing with a membrane pores no larger than 8.0 kDa. An excess of TEV protease was added to the dialysis tubing. The dialysis tubing containing K-Ras^{G12C} and TEV protease was then sealed and incubated overnight in Dialysis Buffer (10 mM HEPES, 50 mM NaCl, 5 mM $MgCl_2$, 10 µM GDP, 0.5 mM 2-ME, 5% glycerol, pH 7.75) at 4°C on a magnetic stir plate. The next day, the SDS-PAGE gel was run to determine purification and TEV-cleavage efficiency. After TEV cleavage was determined to be greater than 80%, the protein was poured over the nickel column once more and the flow through was collected. The column was washed with Dialysis Buffer and 35 µL samples were taken and added to 900 µL of Bio-Rad protein assay dye. The addition of Dialysis Buffer was

stopped once there was no color change in the Bio-Rad protein assay dye. A Shimadzu UV-2501 PC UV-Vis Spectrophotometer was used to measure the absorbance of the protein at a wavelength of 280 nm in a 500 µL quartz cuvette with a 1 cm path length. The protein concentration was then calculated using Beer's Law with the molar absorptivity coefficient for K-Ras^{G12C} being 19,920 $M^{-1}cm^{-1}$. The protein sample was further purified using fast protein liquid chromatography (FPLC) on a Superdex 75 size-exclusion column with Ras FPLC Buffer (50mM HEPES, 150 mM NaCl, 5 mM $MgCl_2$, 15 µM GDP, 0.5 mM 2-ME, pH 7.75). Final purity was assessed by SDS-PAGE gel.

SDS-PAGE. During purification washes/elution, 21 µL samples were taken and 7 µL of reducing dye was added to these samples. The samples were boiled for 3 minutes and loaded onto 15% polyacrylamide gels with a molecular weight marker ranging from 14.4 to 97.4 kDa. The gel was run for 52 minutes at 200V. The gel was stained with coomasie blue and de-stained with 7% acetic acid and 5% ethanol solution.

Nucleotide Loading. Mant-GMPPCP and Mant-GDP were synthesized from stocks of GMPPCP and GDP that were purchased from Jenna Biosciences. The K-Ras^{G12C} was buffer exchanged four times using a 10 kDa cutoff Amicon concentrator tube into loading buffer (20 mM HEPES, 0.25 mM $MgCl_2$, 50 mM NaCl at pH 7.4). The protein was then concentrated down to about 500 µL. A small sample was taken and diluted to a concentration of 10 µM and a volume of 50 µL for later comparison to determine loading efficiency. For Mant-GDP loading, EDTA was added to the remaining protein sample to a concentration of 0.5 mM and Mant-GDP was added to a concentration ratio of K-Ras^{G12C} to Mant-GDP of 1:5. The sample was then nutated at room temperature for 2 hours. For Mant-GMPPCP loading, the remaining protein sample was then added to an Eppendorf tube of 420 µL of Alkaline Phosphatase beads (10 mg Alkaline Phosphatase covalently bound to Sepharose beads, 100 µM $ZnCl_2$, 0.25 mM EDTA, 100 mM $(NH_4)_2SO_4$, 2% glycerol, 0.02 NaN_3 at pH 7.4). Mant-GMPPCP was added to the Eppendorf tube to achieve a final ratio of K-Ras^{G12C} to nucleotide of 1:5. The Eppendorf tube was then placed on a nutator overnight at 4°C.

Mant-nucleotide loading efficiency was measured the next day using a high-performance liquid chromatography (HPLC) machine from Agilent Technologies. A C-18 bonded silica column was used for reverse phase chromatography. The 10 µM sample from the day before and a 30 µL sample from the overnight loading were boiled and spun down for 4 minutes at 13,000 rpm. The solutions of isolated nucleotides were then run on the HPLC column along with 10 µM Mant-GMPPCP, Mant-GDP, and GDP references. Loading was determined to be successful if the overnight loading sample showed an increase in its GMP peak and a decrease in its GDP peak due to Alkaline Phosphatase cleavage. For Mant-GMPPCP loading, the free Mant-GMPPCP should out-compete the bound GMP and bind to the protein. The Mant-GMPPCP peak should then decrease between the sample taken the day before and the sample taken after overnight loading.

After determining that Mant-nucleotide loading was successful, the Eppendorf tube containing the Alkaline Phosphatase beads and K-Ras^{G12C} loaded with Mant-nucleotide was centrifuged for 3 minutes at 13,000 rpm. The supernatant, containing that Mant-nucleotide loaded K-Ras^{G12C}, was then buffer exchanged four times using a 10 kDa Amicon centrifuge tube into Mant-

dissociation buffer (20 mM HEPES, 50 mM NaCl, 5 mM $MgCl_2$ at pH 7.4). The concentration of the protein was then measured similarly to the method above. Then, the sample was stored in a brown Eppendorf tube to protect the Mant fluorophore from photobleaching.

Mant-Nucleotide Exchange Assays. After loading, the Mant-nucleotide loaded K-Ras^{G12C} and GDP loaded K-Ras^{G12C} were buffer exchanged into low magnesium Mant-dissociation buffer (20 mM HEPES, 50 mM NaCl, 0.25 mM $MgCl_2$ at pH 7.4). To a 2.0 mL quartz cuvette with a micro-stir bar, 1.0 mL of low magnesium Mant-dissociation buffer was added. To this cuvette, Mant-loaded K-Ras^{G12C} was added to a final concentration of 1.0 µM and EDTA was added to a final concentration of 0.25 mM. For the SOS-mediated Mant-GDP dissociation assay, SOS^{cat} was added in a 1:1 ratio to K-Ras^{G12C}. The cuvette was then placed in a Perkin Elmer LS-50B Luminescence Spectrophotometer and the assay was started. For the Mant-GDP and SOS-mediated Mant-GDP dissociation assays, free GDP was added to a final concentration of 1mM soon after beginning the assay. For the Mant-GDP and Mant-GMPPCP association assays, free Mant-GDP and free Mant-GMPPCP was added, respectively, to a final concentration of 0.25 µM soon after beginning the assay. Readings were taken at 5 second intervals for 15 or 30 minutes with the excitation wavelength at 395 nm and the emission wavelength at 465 nm. Naringenin was added to subsequent assays to a final protein to naringenin ratio of 1:1, 1:2, 1:5, and 1:10. DMSO was added to the sample to a final composition of 4% DMSO in all assays in order to account for the lower solubility of naringenin in solution.

NMR Data Acquisition. The ^{15}N-labeled K-Ras^{G12C} protein sample was buffer exchanged twice using 10 kDa Amicon centrifuge tubes into NMR buffer (20 mM Tris-Maleate, 50 mM NaCl, 5 mM $MgCl_2$ at pH 6.5). The sample was then concentrated to a volume of 400 µL with a concentration of at least 40 µM protein. Then, about 21 µL of D_2O was added to make the NMR sample a final composition of 5% D_2O. The HSQC spectra acquisition was performed using a Bruker 700 MHz NMR machine using Topshim software. Naringenin was then added to the same sample for a protein to naringenin concentration ratio of 1:1, 1:3, 1:7, 1:12, 1:18, and 1:25. DMSO was added to the sample to a final composition of 4% DMSO in order to increase the solubility of naringenin in solution.

Warhead Reaction. Purified K-Ras^{G12C} was exchanged into dialysis buffer via dialysis to remove excess glycerol from the -20°C storage buffer. EDTA was added to a concentration of 5 mM. 2-mercaptoethanol (2-ME) was added to a 100-fold excess of the protein concentration. UNC-5700, dissolved in 100% DMSO, was added to 100-fold excess of the protein concentration, as well. Additional DMSO was added, up to a concentration of 4%, to facilitate dissolution of UNC-5700 into solution. The sample was left at room temperature for two hours. The sample was buffer exchanged into dialysis buffer to remove unreacted UNC-5700.

ABD-f Assay. Ligated K-Ras^{G12C} was buffer exchanged into reducing buffer via four consecutive runs through 10 kDa Amicon tubes. The sample was then buffer exchanged into non-oxidizing buffer (no reducing agent) which was sparged for 30 minutes with nitrogen gas prior to buffer exchange. The sample was concentrated to a final concentration of 20 µM and a 100 µL sample was added to into one well of a 96-well black fluorimeter tray. To this, 100 µL of 200 µM (4-fluoro-7-sulfamoylbenzofurazan) ABD-f was added, mixed, and quickly inserted into the fluorimeter.

Results

Unlabeled K-Ras^{G12C} was purified with a high yield and purity (Figure 1). ^{15}N-labeled K-Ras^{G12C} was purified with a similar yield and purity (data not shown).

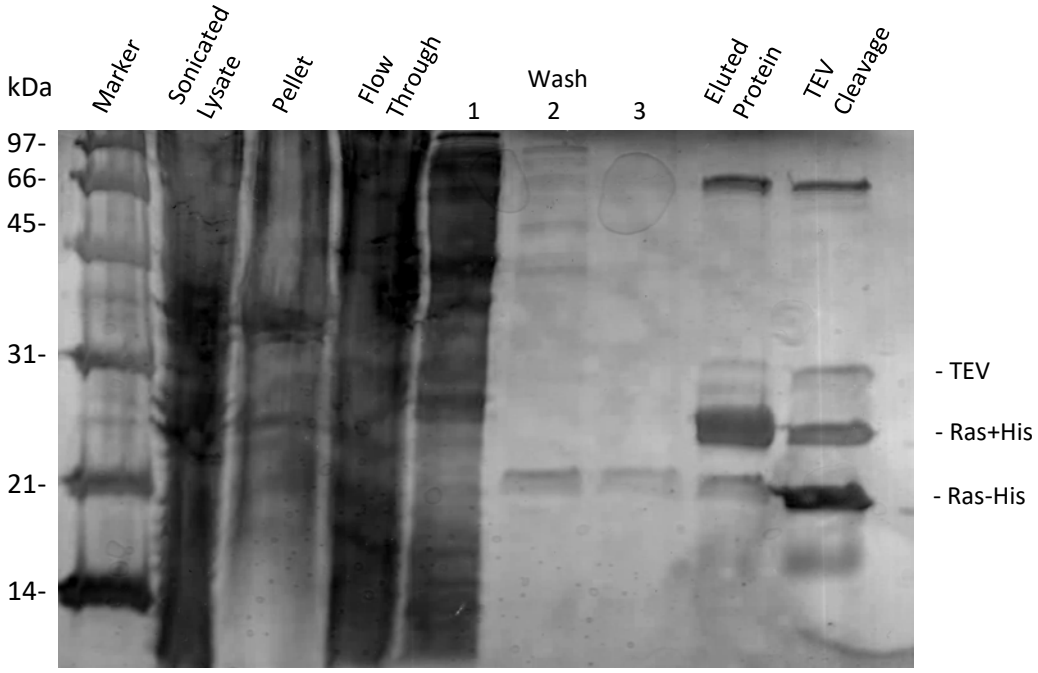

Figure 1. SDS-PAGE analysis of K-Ras^{G12C} purification. The bands at ~20kDa, ~25kDa, and ~31kDa correspond to K-Ras^{G12C}, His-tagged K-Ras^{G12C}, and TEV, respectively. Overnight TEV cleavage was repeated as needed to cleave additional tagged K-Ras^{G12C} that was left uncleaved in the TEV Cleavage lane. The K-Ras^{G12C} protein was purified further via fast protein liquid chromatography (FPLC) on a Superdex 75 column.

Rates of Mant-GDP intrinsic dissociation, SOS mediated Mant-GDP dissociation, Mant-GDP association, and Mant-GMPPCP association were measured by fluorescence-based assays. The first two assays were performed for 30 minutes and measurements were taken in 5 second intervals, resulting in 360 measurements of fluorescence per assay. The second set of association assays were performed for 15 minutes and measurements were taken in 5 second intervals, resulting in 180 measurements of fluorescence per assay. Association of Mant-nucleotide to Ras caused an increase in fluorescence by about 40%, while its dissociation lead to a decrease in fluorescence by about 40%. The Mant-nucleotide fluorescence data was normalized and transferred to Graphpad Prism Software where the dissociation and association rates were determined. The rates of nucleotide dissociation and association was then graphed. An increase in intrinsic rate of Mant-GDP dissociation was observed with an increase in the relative concentration of naringenin to K-Ras^{G12C} (Figure 2: a and c). SOS-mediated Mant-GDP dissociation rates were not significantly affected by increasing the relative concentration of naringenin (Figure 2: b and d). Mant-GDP association rates initially increased with a ratio of 1:1 and 1:2 K-Ras^{G12C} to naringenin. An addition of more naringenin resulted in a decreased in the association rate of Mant-GDP (Figure 2: e and g). Mant-GMPPCP association initially increased

upon the addition of naringenin but plateau at 1:2 and 1:5 ratios of protein to naringenin (Figure 2: f and h).

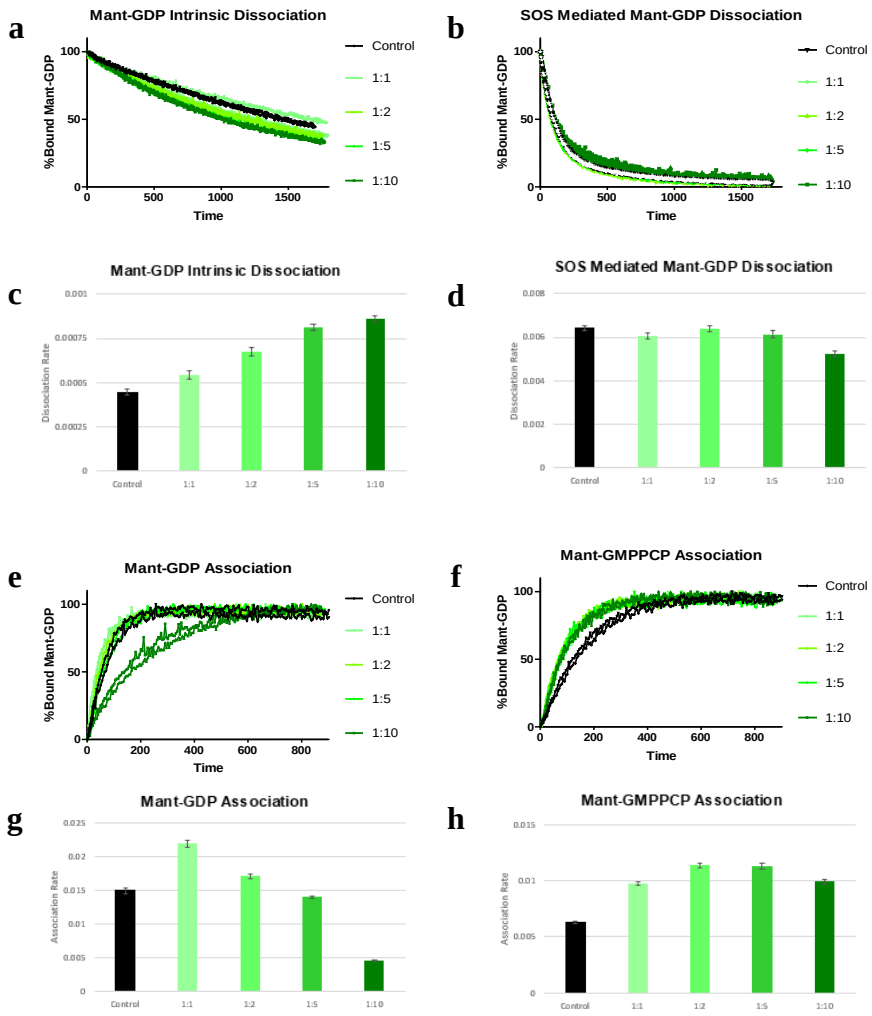

Figure 2. Mant-nucleotide exchange assays of K-Ras^{G12C} in the absence and presence of increasing concentration of naringenin. **a-d.** The black dissociation curves corresponding to the "Control" assays are samples without naringenin. The green dissociation curves correspond to assays that contain a 1:1 to 1:10 protein to compound ratio, with the ratio increasing with the darkening of the green curves. **e-h.** The plots of the K_d values associated with each assay correspond with the same color scheme. Errors were determined by standard error after fitting to a one-phase exponential decay (n=4).

After acquiring the HSQC spectra of K-Ras^{G12C}, peak backbone assignments for each amino acid of K-Ras^{G12C} were made. The Sparky NMR program was used to measure the peak assignments of each peak. The CSPs were calculated using Equation 1, and the CSPs were plotted against the naringenin concentration in Graphpad Prism software. A one-site specific binding curve fit was plotted and the dissociation rates were calculated by the program. CSPs at residues T74, G75, G60, G10, an unknown residue, and L6 were chosen for analysis due to their significant CSPs (Figure 3: b-j). The dissociation constants that were measured were found to be within a low millimolar or high micromolar range. The dissociation rate of residue 5 was not included due to a poorly fit curve.

K-Ras^{C118S} (1mM) was co-crystallized with excess naringenin (5mM) and then soaked in solution with 10 mM naringenin. Crystals were grown under several conditions and the crystal structure was solved, courtesy of Dr. Hengming Ke (Figure 4, 5). A high-resolution crystal structure of K-Ras^{C118S} (1.6 Å resolution) with the

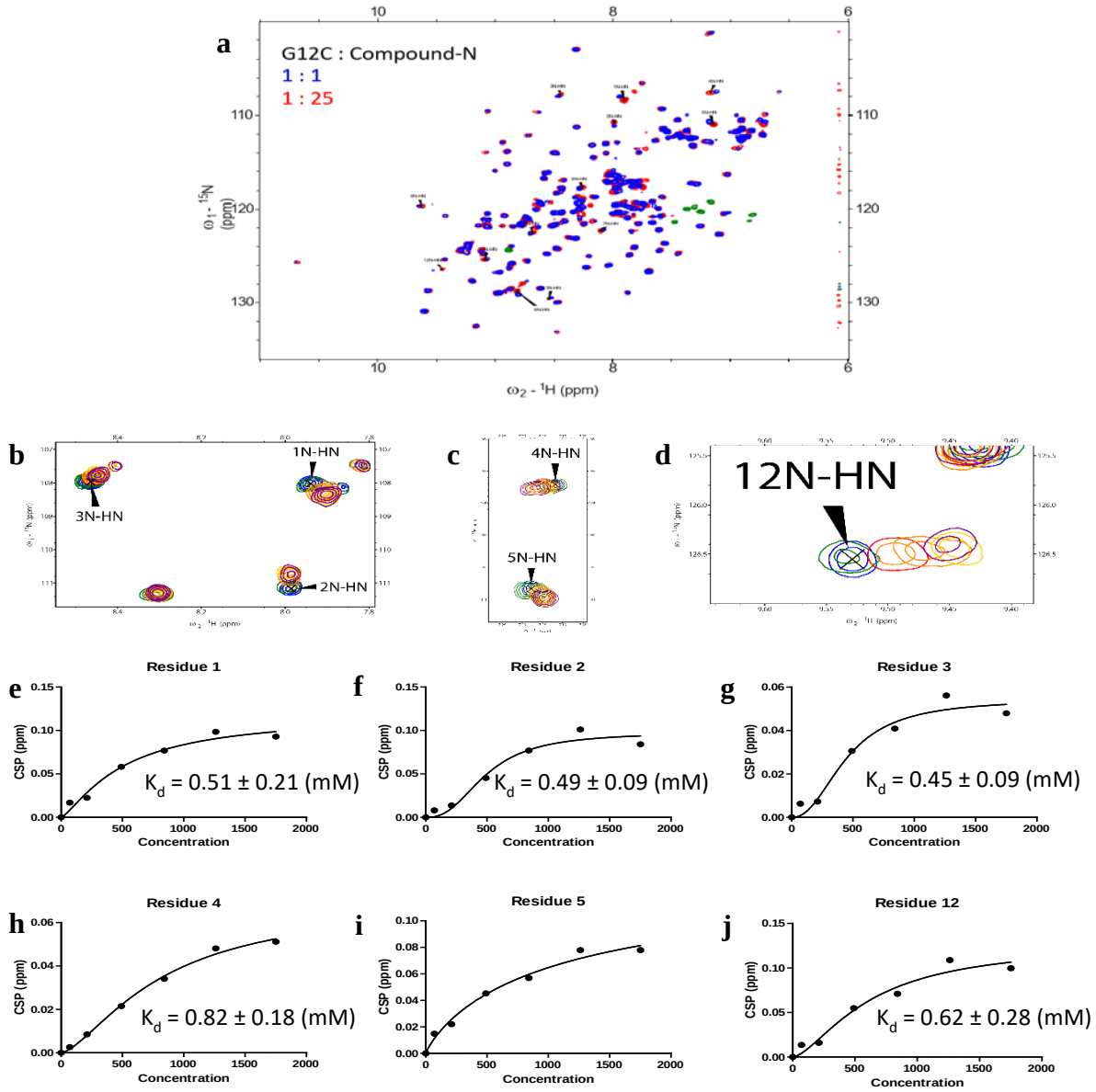

Figure 3. Chemical shift perturbations of K-Ras^{G12C} residues upon naringenin titration. **a.** An N^{15} NMR sample of K-Ras^{G12C} was titrated with an incremental addition of naringenin, from a 1:1 concentration ratio of K-Ras^{G12C} to Compound N to a 1:25 concentration ratio. The HSQC spectra of the 1:1 ratio and 1:25 ratio were overlaid, displaying multiple chemical shift perturbations (CSPs) corresponding to the increase in relative naringenin concentration. **b-d.** Particular residues with CSPs that trend with an increasing naringenin concentration were chosen to measure the dissociation constant (K_d) of naringenin at those residues. The colors blue, green, red, orange, yellow, and violet correspond to the following ratios of K-Ras^{G12C} concentration to Compound N concentration, respectively: 1:1, 1:3, 1:7, 1:12, 1:18, and 1:25. **e-j.** Residues 1-5 and 12 correspond to the following K-Ras^{G12C} residues, respectively: T74, G75, G60, G10, unknown, and L6. The dissociation rate for Residue 5 was omitted due to a poorly fitted curve.

structure similar to that previously published.[3] The electron-density of naringenin was not found

in the structure, likely due to weak binding.

UNC-5700 was successfully ligated to K-Ras^{G12C}. The ligation was tested via multiple ABD-f assays (Figure 6). The lack of ABD-f fluorescence after warhead ligation indicated that cysteine-12 was no longer available to be ABD-f reactive. The low fluorescence would only be possible if cysteine-12 was ligated to the warhead or if it was oxidized. The G12C control plot, which was prepared from the same sample that was used for ligation, indicated that the low fluorescence of G12C + Warhead runs were not due to an oxidation of cysteine-12. The wildtype K-Ras^{C118S} run was used as a control to show that the only available cysteine on K-Ras^{G12C} is cysteine-12. The cysteine-light K-Ras constructs were confirmed to have no other reactive cysteines. Mant-nucleotide assays were performed on UNC-5700 ligated K-Ras^{G12C} (Figure 7). The non-ligated K-Ras^{G12C} was measured to have a relative dissociation rate (K_{GTP}/K_{GDP}) of 1.69 s^{-1}, while the UNC-5700 ligated K-Ras^{G12C} was measured to have a slightly lower relative dissociation rate of 1.63 s^{-1}.

1

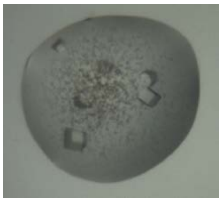

2

3

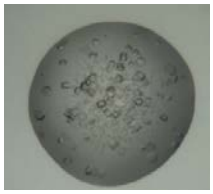

4

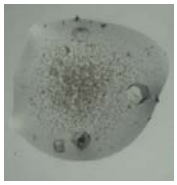

Drop Conditions [50% C118S+Ligand, 0.2µl]

Type	Conc	Units	Name	pH	Group	Source
Crystallant	1.8	M	NaH2/K2H Phosphate	8.2	Buffer	MCSG 2.B4

Drop Conditions [33.33% C118S+Ligand, 0.3µl]

Type	Conc	Units	Name	pH	Group	Source
Crystallant	0.2	M	sodium chloride		Salt	MCSG 3.H5
	1	M	sodium citrate		Salt	MCSG 3.H5
	0.1	M	Tris	7	Buffer	MCSG 3.H5

Drop Conditions [50% C118S+Ligand, 0.2µl]

Type	Conc	Units	Name	pH	Group	Source
Crystallant	1.2	M	sodium citrate		Salt	MCSG 4.C2
	0.1	M	Tris	8.5	Buffer	MCSG 4.C2

Drop Conditions [50% C118S+Ligand, 0.2µl]

Type	Conc	Units	Name	pH	Group	Source
Crystallant	0.2	M	sodium chloride		Salt	MCSG 2.G3
	0.4	M	sodium dihydrogen phosphate		Salt	MCSG 2.G3
	1.6	M	di-potassium hydrogen phosphate		Salt	MCSG 2.G3
	0.1	M	imidazole	8	Buffer	MCSG 2.G3

Figure 4. Crystallization conditions of K-Ras^{C118S}. The conditions for drops 1-4 correspond in chronological order of the buffer conditions from top to bottom.

HSQC was performed on K-Ras^{G12C} and on ARS-853 ligated protein (Figure 8). Chemical shift perturbations were found across most of the HSQC spectra due to ARS-853 ligation. The chemical shift peaks experienced little broadening. HSQC was also performed on K-Ras^{G12C} in the presence of excess naringenin and K-Ras^{G12C} ligated to UNC-5700 (Figure 9). The presence of naringenin induced moderate chemical shift perturbations and broadening in peaks corresponding to the switch-I and switch-II regions of K-Ras. The UNC-5700 ligated K-Ras^{G12C} showed similar chemical shift perturbations. High Ambiguity Driven protein-protein DOCKing (HADDOCK) modeling was performed by Guowei Yin on K-Ras^{G12C} to dock naringenin within the allosteric pocket, and naringenin adopted multiple conformations within the allosteric pocket (Figure 10).[7]

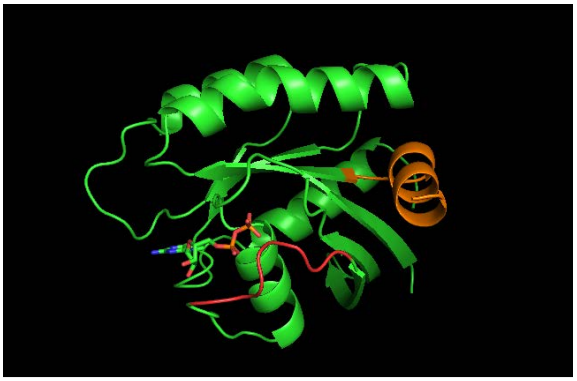

Figure 5. Crystal structure of K-Ras^{C118S} in the presence of excess naringenin. The naringenin did not induce changes in the crystal structure of K-Ras^{C118S}.
Red: switch-I
Orange: switch-II

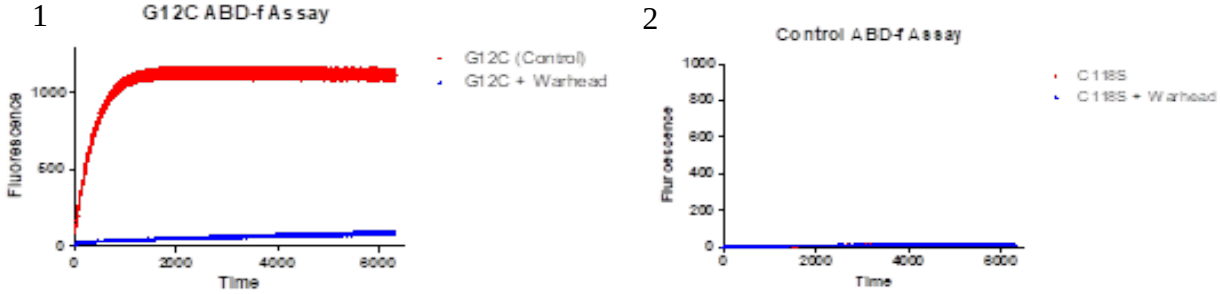

Figure 6. ABD-f assays of ligated K-Ras^{G12C} compared to controls. Plot 1: UNC-5700 was ligated to K-Ras^{G12C} and compared to non-ligated K-Ras^{G12C}. Plot 2: K-Ras^{C118S} was incubated with UNC-5700 in identical conditions and serves as a negative control for the ABD-f assays. Errors were determined by standard error (n=3).

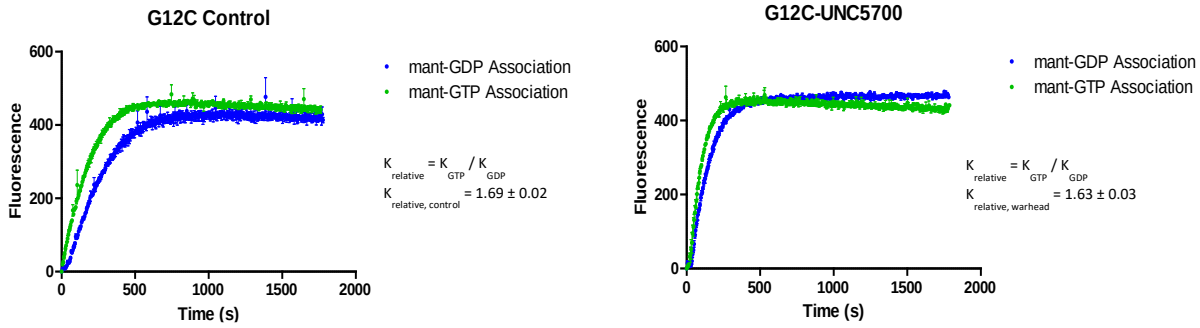

Figure 7. Mant-nucleotide association assays. Each assay was performed under identical conditions in triplicate. The ratio of the rate of association between Mant-GTP and Mant-GDP association was calculated. Errors were determined by standard error (n=3).

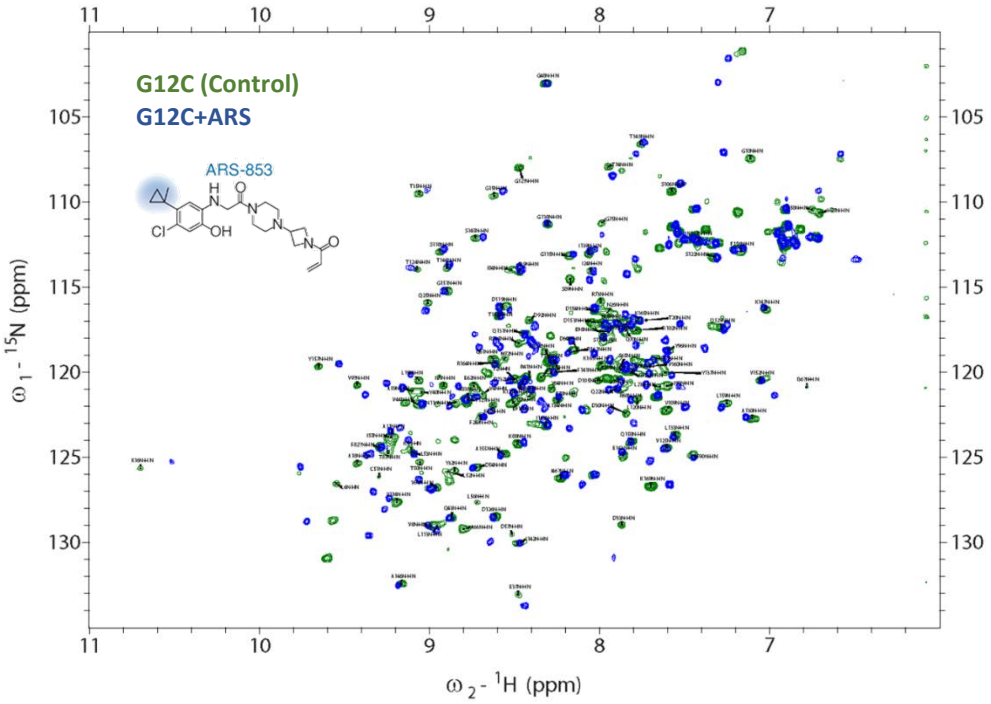

Figure 8. HSQC of K-Ras^{G12C} with and without ligation by ARS-853. Significant CSPs were found throughout the spectra due to ARS-853 binding.

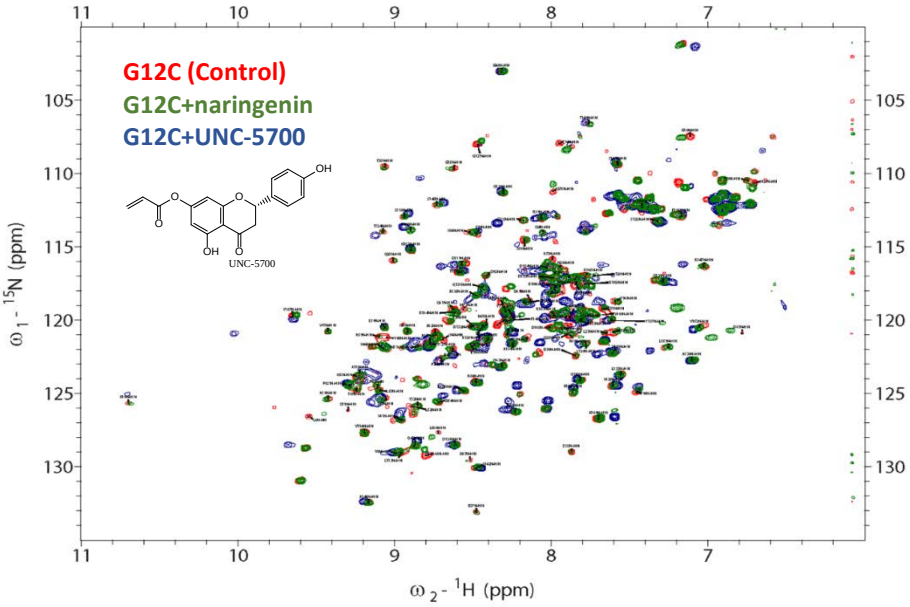

Figure 9. HSQC of K-Ras^{G12C}, K-Ras^{G12C} with excess 1:25 molar ratio naringenin, and K-Ras^{G12C} ligated to UNC-5700. CSPs from UNC-5700 were found mostly at switch-II residues and are similar to CSPs from the naringenin titration.

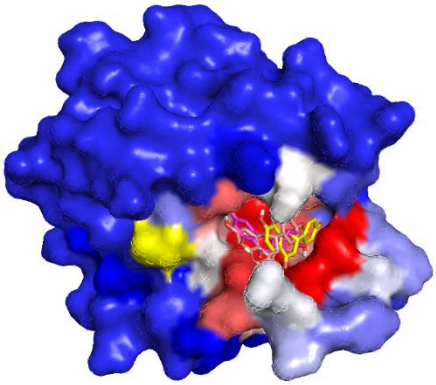

Figure 10. HADDOCK model of K-Ras^{G12C} – naringenin docking in the allosteric pocket. HADDOCK modeling was performed by Guowei Yin.

K-Ras^{G12C}: yellow – Cys12; red – allosteric pocket; blue – outside surface; white – switch-II region

Naringenin: yellow, magenta, pink – multiple conformations within the allosteric pocket

Discussion

From this study, the expression and purification of K-Ras^{G12C} was optimized. The BL21(DE3) RipL cell line was determined to be the most efficient competent cells to overexpress the protein. The optimal growth conditions for stimulating the overexpression of K-Ras^{G12C} while preventing oxidation were also found. Changes were made in the procedure to include enough reducing agent throughout the purification process to keep K-Ras^{G12C} in its more stable, non-oxidized form. Retaining the activity of the reactive cysteine will be imperative for experiments in the future that will depend on the ligation of naringenin to the cysteine.

The experiments performed in this study indicated that naringenin does induce changes in overall guanine nucleotide exchange and binding affinity (Figure 2). An increase in the dissociation rate of Mant-GDP in the presence of naringenin is indicative of naringenin affecting the exchange dynamics and/or decreasing binding affinity of GDP to K Ras^{G12C} (Figure 2: a and c). This conclusion is also supported by data from our Mant-GDP association assays (Figure 2: e and g). The overall decrease in the GDP association rate indicated that naringenin slightly affected the GDP binding affinity on K-Ras^{G12C}. The lack of change found in SOS mediated nucleotide exchange suggested that naringenin does not affect GEF binding (Figure 2: b and d). However, the increase observed in the Mant-GMPPCP association rate is indicative of an increase in GMPPCP binding affinity due to naringenin binding (Figure 2: f and h). A possible reason for this increase in the rate of exchange between GDP and Mant-GMPPCP is that naringenin affected GDP binding more than GMPPCP binding, causing K-Ras^{G12C} to prefer its activated, GTP-bound state over its inactivated, GDP-bound state. This change directly opposes changes in GTP binding by K-Ras^{G12C} inhibitors. However, the changes in GTP association rates are

insignificant compared to the expected change of an effective K-Ras^{G12C} inhibitor. Interpreting naringenin as a small molecule that increases or decreases nucleotide association/dissociation rates is not appropriate due to its weak binding affinity to K-Ras^{G12C}.

From our HSQC data, the majority of CSPs that were caused by naringenin were found to be in the switch-II region of K-Ras^{G12C}. The titration of naringenin into our NMR sample caused an increase in CSPs (Figure 3: b-d). The calculated dissociation rates were found to be on a low millimolar or high micromolar scale (Figure 3: e-j). This was interpreted to mean that naringenin has a relatively low binding affinity to the switch-II region. Conversely, the binding affinities of GDP and GTP are within the picomolar scale. This large difference in the binding affinity of naringenin to K-Ras^{G12C} compared to the binding affinities of the guanine nucleotides could indicate that naringenin cannot not bind very tightly to the allosteric pocket located in the switch-II region of K-Ras^{G12C} due to its inability to compete with nucleotide binding. Nucleotide exchange may have induced conformational change in the switch-II region even with the presence of naringenin. However, the naringenin was still able to impede GDP exchange but not the exchange of GDP for GMPPCP. The low binding affinity of naringenin does not allow it to act as a sufficient inhibitor of the GMPPCP binding, which has extremely tight picomolar binding affinity.

Together, the Mant-nucleotide exchange and NMR data show that naringenin binds weakly to K-Ras^{G12C}, and that this weak binding within the switch-II region does not inhibit the activation of K-Ras^{G12C}. However, the NMR data shows that the saturation of K-Ras^{G12C} by naringenin requires a relative concentration of K-Ras^{G12C} to naringenin to be at least 1:25. In future Mant-nucleotide exchange experiments, the relative concentration of naringenin will be increased to achieve this saturation to confirm the effects of naringenin on nucleotide exchange. The dissociation and association rates measured for SOS mediated Mant-GDP dissociation and Mant-GMPPCP association do not show a clear trend with the addition of naringenin to a concentration ratio of 1:10. These experiments should be repeated with the concentration ratios expanded to at least 1:25 to correspond with the NMR data.

The acrylate group addition made to naringenin (UNC-5700) successfully ligated cysteine-12 of K-Ras^{G12C}, confirmed via ABD-f assays (Figure 6). The lack of fluorescence observed by the ligated protein was due to the loss of reactivity of cysteine-12, the only reactive and exposed cysteine of K-Ras^{G12C} (Figure 6, Plot 1). ABD-f normally fluoresces upon reduction or upon binding to reduced, activated thiols. The negative control confirms that UNC-5700 does not ligate any reactive thiols of the wildtype protein, K-Ras^{C118S} (Figure 6, Plot 2).

Though the issues of naringenin's affinity to the switch-II allosteric pocket are solved by the addition of an acrylate group to facilitate irreversible ligand binding, the orientation of allosteric-binding portion of UNC-5700 does not allow it to fit with low steric-hindrance within the allosteric pocket like the ligand ARS-853 (Figures 8 and 9). Accordingly, the relative binding of GTP and GDP to UNC-5700 bound K-Ras^{G12C} was not expected to be greatly affected (Figure 7). Both GTP and GDP have picomolar binding affinities to Ras, while naringenin was found to have micromolar binding affinity, limiting its ability to compete with nucleotide binding.

ARS-853 ligation causes significant CSPs throughout the HSQC spectrum, suggesting that its binding within the switch-II allosteric pocket manifests protein-wide changes in conformation (Figure 8). Its ability to stifle GTP-binding suggests that the conformation of the GTP-binding site, switch-I, switch-II, and/or the p-loop of Ras may alter by its ligation.[3] These conformational differences are not present within the spectra of UNC-5700 ligated K-Ras^{G12C} (Figure 9). Significant CSPs are found within the switch-II region, but other peak changes are characterized by their apparent broadening. The broadening of peaks suggests that UNC-5700 assumes several conformations and may be moving in and out of the allosteric pocket. The HADDOCK model reflects that more restraints (CSP data and potential function restraints) are needed to specify the binding mode of naringenin within the allosteric pocket (Figure 10). This inability to bind strongly within the allosteric pocket reflects back on the relatively weak binding affinity of naringenin compared to GTP and GDP (Figure 3).

Though the data from these experiments do not conclusively reveal the effect of naringenin and UNC-5700 on the activation of K-Ras^{G12C}, they do provide important information on the future modifications that should be made to UNC-5700. This study shows that naringenin seems to weakly bind to the switch-II region of K-Ras^{G12C}. With this information, we can affectively modify naringenin by adding various chemical groups that would increase its binding affinity to that allosteric pocket. For example, different hydrophobic chemical groups can be added to naringenin to increase its affinity within the allosteric pocket that is made up of several hydrophobic residues. Future work with naringenin can lead to a new treatment for non-small cell lung carcinomas. Furthermore, the expansion of Ras inhibitor drug design can be explored through other naringenin-like drugs/metabolites that are already of clinical use. Selective estrogen receptor modulators (SERMs) provide another scaffold onto which more irreversible ligands may be synthesized by K-Ras^{G12C} testing. NMR data has verified that several SERMs bind to the same allosteric pocket of K-Ras as naringenin (data not shown). Other modifications, such as cysteine-12 oxidation, may also have effects on K-Ras^{G12C} nucleotide binding, because of the residues proximity to the nucleotide binding site. Lastly, targeting the switch-II region of Ras may prove beneficial for Ras drug discovery due to the variability of the switch-II conformation across Ras isoforms. N-Ras and H-Ras have different switch-II conformations, meaning that similar inhibitors to the ones discussed here can be developed with isoform-specificity. Overall, future research into this new means of Ras drug development can lead to a new generation of Ras inhibitors for cancer treatments involving other Ras mutations.

Supplemental Figures:

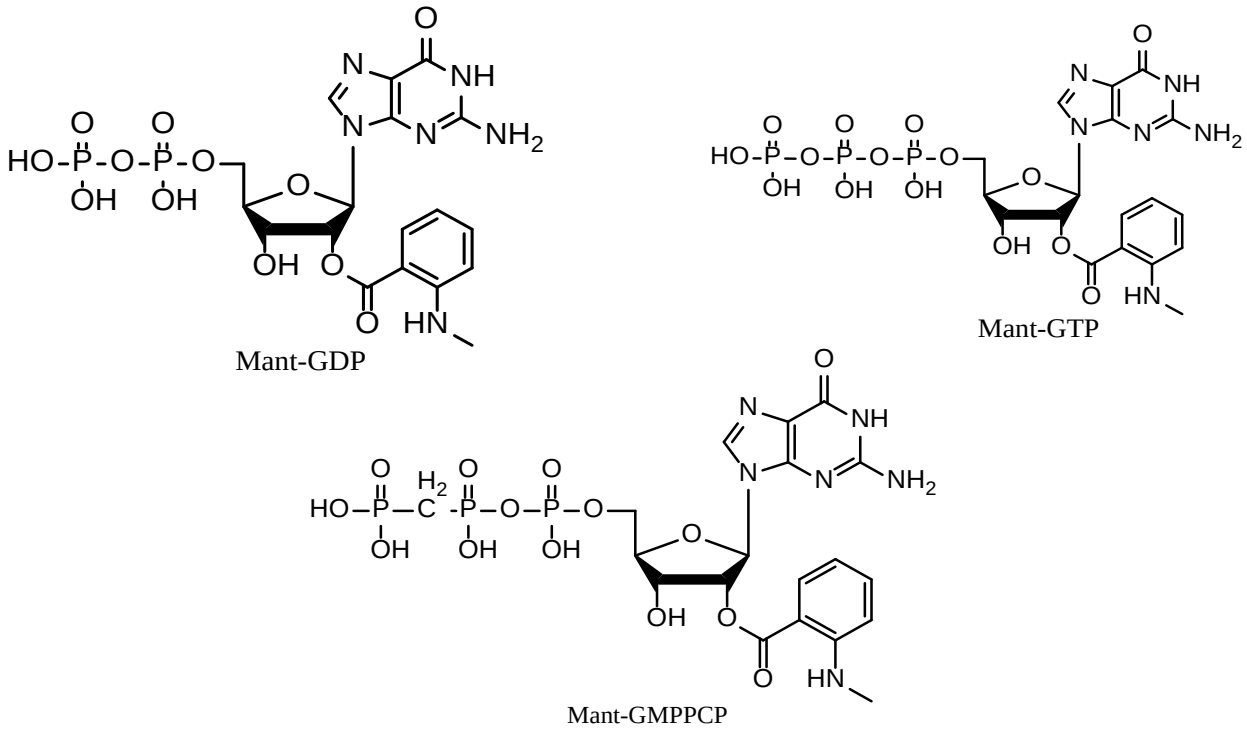

Supplemental Figure 1. Structures of Mant-fluorescent nucleotide analogues.

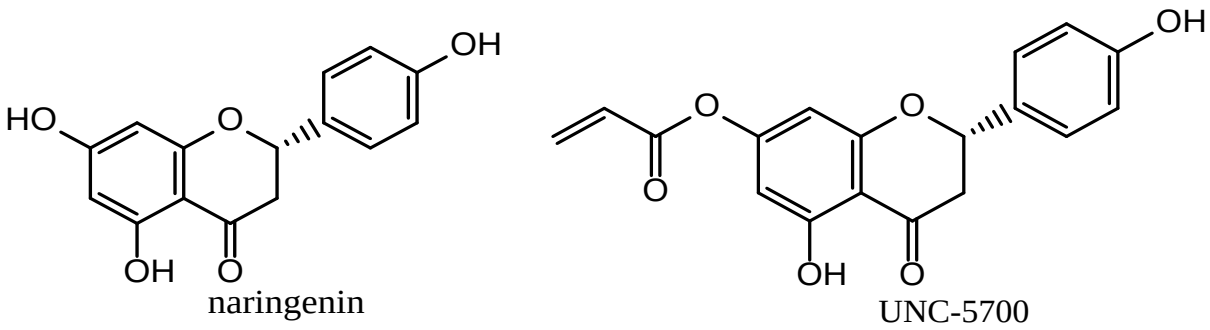

Supplemental Figure 2. Structures of naringenin and UNC-5700.

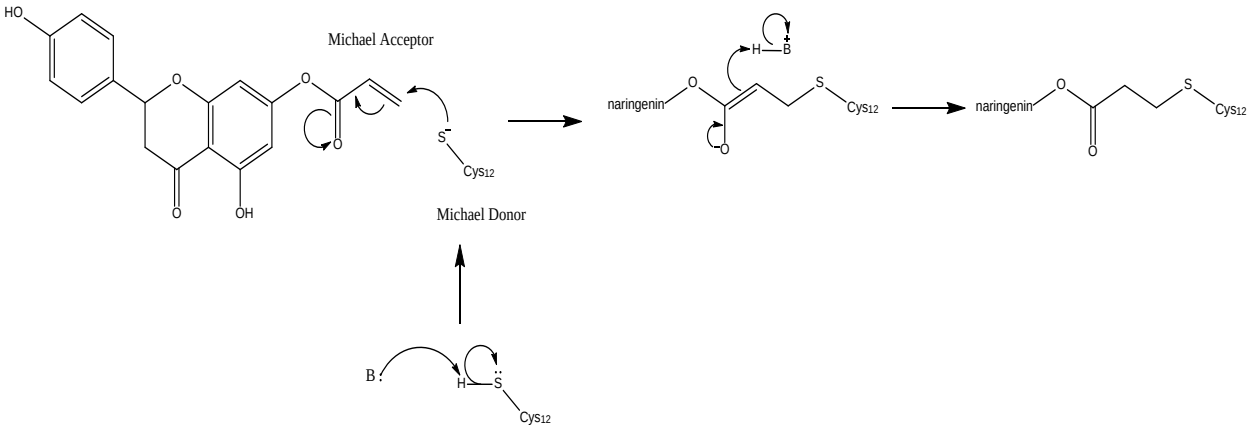

Supplemental Figure 3. Mechanism of UNC-5700-cysteine-12 reaction.

References

1. Simanshu, D.K. et al. “RAS Proteins and Their Regulators in Human Disease” *Cell.* 170 (2017): 17-33.
2. Forbes, S.A. et al. “COSMIC: Mining complete cancer genomes in the Catalogue of Somatic Mutations in Cancer.” *Nucleic Acids Res.* 39 (Database issue) (2011): D945–D950.
3. Ostrem, Jonathan M. et al. “K-Ras(G12C) Inhibitors Allosterically Control GTP Affinity and Effector Interactions.” *Nature* 503.7477 (2013): 548–551.
4. Janes, Matthew R. et al. “Targeting KRAS Mutant Cancers with a Covalent G12C-Specific Inhibitor.” *Cell* 172 (2018): 578-589.
5. Plotnikov, Alexander et al. “The MAPK cascades: Signaling components, nuclear roles and mechanisms of nuclear translocation.” *Biochimica et Biophysica Acta (BBA) - Molecular Cell Research*. 1813(9) (2011): 1619-1633.
6. Cox, A.D., Der, C.J. “Ras history: The saga continues.” *Small GTPases*. 1 (2010): 2-27.
7. Dominguez, C. et al. “HADDOCK: A Protein-Protein Docking Approach Based on Biochemical or Biophysical Information.” *J. Am. Chem. Soc.* 125 (2003): 1731-1737.